Supporting Information

Flexible, shape-editable wood-based functional materials with acetal linkages

Yi Tan[a,c], Kaili Wang[b], Shanshan Gong[a], Hui Chen[a], Youming Dong[b], Qiang Gao[a], Chengguo Liu[c]*, Jianzhang Li[a]*

[a] *State Key Laboratory of Efficient Production of Forest Resources, MOE Key Laboratory of Wooden Material Science and Application, Beijing Key Laboratory of Wood Science and Engineering, Beijing Forestry University, Beijing 100083, China*

[b] *Co-Innovation Center of Efficient Processing and Utilization of Forest Resources, College of Materials Science and Engineering, Nanjing Forestry University, Longpan Road No.159, Xuanwu District, Nanjing, 210037, China*

[c] *College of Chemical Engineering, Nanjing Forestry University, Longpan Road No.159, Xuanwu District, Nanjing, 210037, China*

[*] *Corresponding author.*

E-mail address: liuchengguo@njfu.edu.cn (C. Liu); lijzh@bjfu.edu.cn (J. Li).

Contents

1. Experimental section

1.1 Materials and chemicals

Balsa wood (*Ochroma pyramidale*) with oven-dried densities of 110.23 ± 0.04 mg/cm^3 was procured from Zhuhai Dechi Technology Co., Ltd., China. Glacial acetic acid (CH_3COOH) was purchased from Tianjin Fuchen Chemical Reagent Co., Ltd., China. Styrene monomer (SM, 99%) was purchased from Xiya Chemical Technology (Shandong) Co., Ltd., China. 2-hydroxyethyl methacrylate (HEMA, 96%), 2-ethylhexyl methacrylate (EMA, 99%), and lauroyl peroxide (LPO, 98%) were purchased from Shanghai Macklin Biochemical Co., Ltd., Shanghai, China. Sodium chlorite ($NaClO_2$, 80%), 1,4-Cyclohexanedimethanol divinyl ether (CDE, 98%), octadecyl acrylate (OA, 97%), and benzoyl peroxide (BPO, 97%) were purchased from Heowns Biochemical Technology Co., Ltd., Tianjin, China. All chemicals were used as received without further purification and treatment.

1.2 Wood delignification treatment

Balsa wood (NW) was sawn into different dimensions in two directions and immersed in the $NaClO_2$ aqueous solution (1 wt %) at 85 °C for several hours, and the pH of solution was adjusted to be 4.6 using CH_3COOH. The treatment solution was exchanged every 8 h. Consequently, the delignified wood skeletons (WS) were rinsed with boiling water to remove residual chemicals, and DW was obtained after freeze-drying. The thickness of the samples in the experiment was 2 mm.

1.3 Fabrication of flexible editable wood composite

Firstly, the precursor acetal-cased network (AN) mixture was prepared by mixing SM (60 mmol), HEMA (5mmol), EMA (3.5mmol) and CDE (3 mmol) under ice bath and ultrasonic treatment, in which the radical initiators LPO and BPO were 0.3 mmol, and the OA was added with 1 wt.% for

defoaming. The SM and EMA were **hydrophobic**,[1, 2] the 2-hydroxyethyl methacrylate (HEMA) was **hydrophilic**.[3] The 1,4-cyclohexanedimethanol divinyl ether (CDE) exhibited the surface tension of 72.2 mN/m at 21 °C and water solubility 0.024 g/l at 20 °C according to the information of basic physical and chemical properties at 406171 (sigmaaldrich.cn).

After the mixture was heating at 80 °C for 30 min, the WS was impregnated in the mixture and degassed under 300 Pa for 10 min at ambient temperature, followed by negative pressure releasing. After impregnation, the impregnated wood composite was sandwiched by two glass slides with PTFE spacer in between, and then it was cured under gradually heating from 90 °C, 120 °C to 150 °C for 2h, 2h, and 3 h, respectively. Finally, the ATW was obtained after cooling at ambient temperature.

1.4 Characterization

The density was determined by the mass and volume of samples. Field-emission scanning electron microscopy (FE-SEM, Hitachi S-4800), equipped with an attached energy-dispersive X-ray spectrometer (EDX, Horiba EX-350) was used to characterize the morphology and structure of samples, at an accelerating voltage of 5.0 kV. CT The contents of the wood main component (cellulose, hemicellulose, and lignin) were measured by two-step sulfuric acid hydrolysis[4]. The chemical components analysis of the samples was performed by attenuated total reflectance Fourier transform infrared spectroscopy (ATR-FTIR, Nicolet 6700) with an ATR diamond crystal, as well as the nuclear magnetic resonance spectrometer (Avance III 500). The transmittance and haze were measured with a light-diffusion system (EEL 57D) according to ASTM D1003 “Standard Method for Haze and Luminous Transmittance of Transparent Plastics”, which is defined as (eq. 1)[5]:

$$Haze = \left(T_4/T_2 - T_3/T_1\right) \times 100\% \quad (1)$$

where T_1 refers to the incident light, T_2 refers to the total light transmitted by the sample, T_3 refers to the light scattered by the instrument and T_4 refers to the light scattered by the instrument and specimen[6].

The intensity distribution of the scattered light at different angles was characterized by an

illuminometer, with a detector area of 1 × 1 cm^2. Differential scanning calorimetric (DSC) measurement was carried out on a TA Q2000 differential scanning calorimeter (Waters) under an N_2 atmosphere in the temperature range of -10~200 °C at a heating rate of 10 °C/min. Dilatometry experiment was conducted on a TMA Q400EM apparatus in tension mode. Under a N_2 atmosphere, the sample was heated from -50 °C to 250 °C at a rate of 5 °C/min, and the length change was measured while small constant force (20 mN) was exerted to avoid bending. Thermogravimetric analysis (TGA) was performed using a TA Q5 (Waters) instrument in the temperature range of 50 °C~600 °C at a heating rate of 10 °C/min in a N_2 atmosphere. The thermal conductivities of the samples with sizes of 25 × 25 × 3 mm^3 were measured using a Hot Disk (TPS 2500S) Thermal Constant Analyzer at 25 °C. Tensile curves and three-point bending curves were recorded on a universal mechanical test machine (Instron 3365) with 5 mm/min strain rate, and the length, width, thickness of samples was 70 × 100× 2 mm^3, respectively.

1.5 Shape recovery and edition

The shape restorability of obtained ATW was quantitatively characterized via bending transformation process. The size of strips was 70 ×100 × 2 mm^3, of which the two ends were bent to 0 ° at 40 °C and cooled to 0 °C to fix the shape. The bending angle change values at different temperatures and times were recorded during the shape transformation process. The shape recovery ratio (R_r) was calculated, which is defined as (eq. 2):

$$R_r = (\theta_r/180) * 100\% \quad (2)$$

where θ_r represents the bending angle after the recovery phase at a certain temperature for a certain amount time.

The shape edition ability of resultant ATW was verified by exerting an external force on TW at 80 °C for 10 min, followed by gradually cooling to ambient temperature and fixing rapidly at 0 °C, to form a reprocessed permanent shape.

2. Figures and Tables

Fig. S1

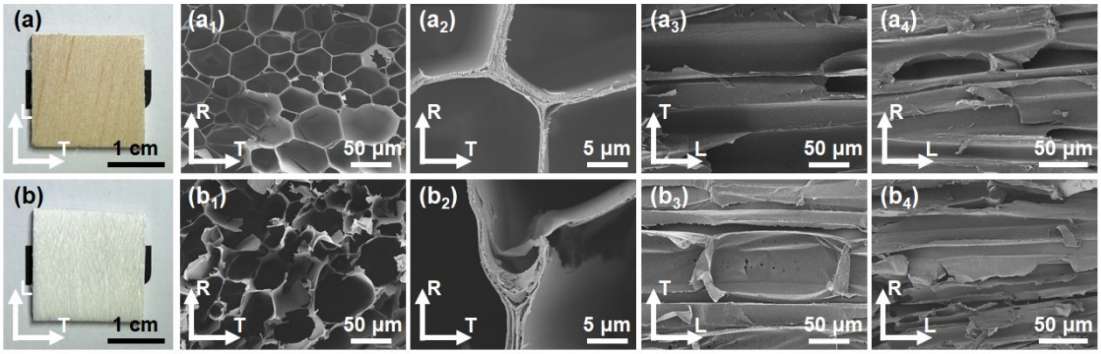

Fig. S1 (a, b) Photograph of NW and WS. (a_1- a_4, b_1- b_4) Transverse, radial, and tangential SEM images of NW and WS.

Fig. S2

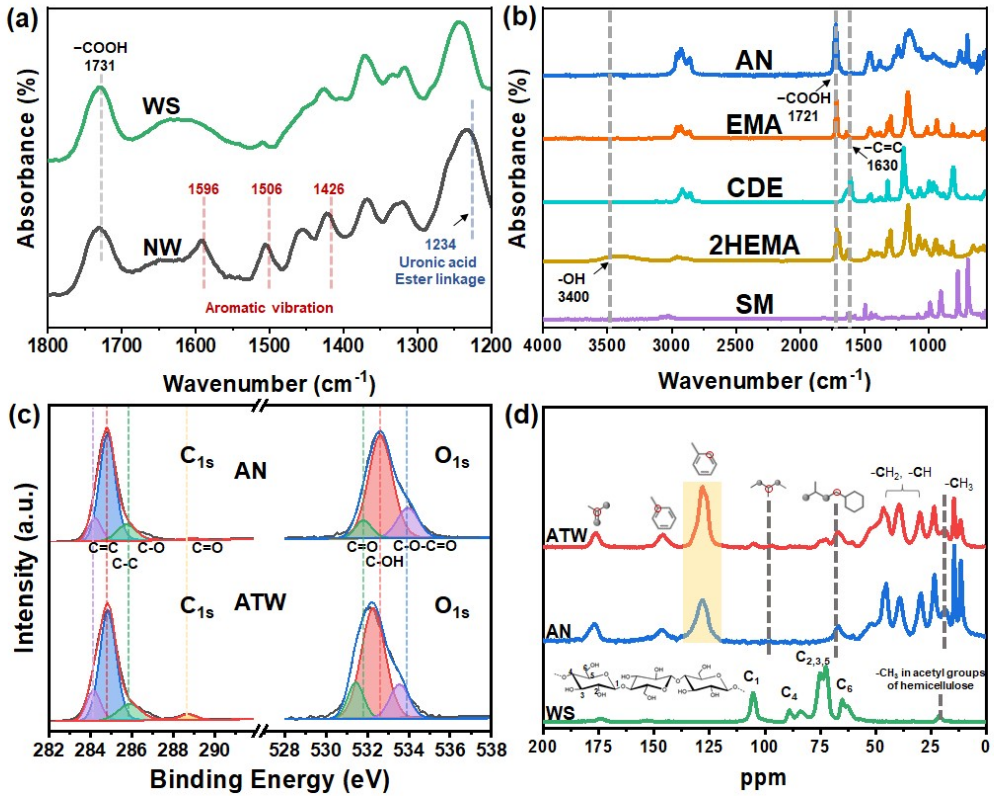

Fig. S2 (a) Locally amplified FTIR spectrum of WS and NW. (b) FTIR spectrum of AN, EMA, CDE, HEMA and SM. (c) XPS spectra of AN and ATW. (d) ^{13}C NMR spectra of WS, AN and ATW.

Table S1

Table S1. Peaks of XPS spectra of ATW and AN.

Element	Assigned groups	Peak value in ATW (eV)	Peak value in AN (eV)
C	C=C	284.18	284.24
	C-C	284.88	284.85
	C-O	285.93	285.79
	C=O	288.78	288.96
	C-O-C=O	533.58	533.98
O	C-OH	532.32	532.67
	C=O	531.48	531.85

Fig. S3

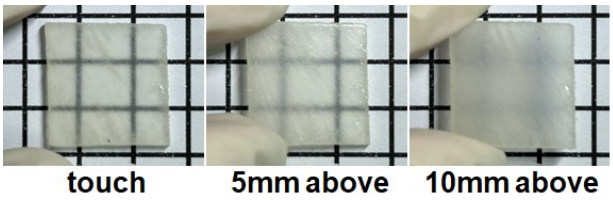

Fig. S3 Digital images of T-ATW positioned above the checkerboard pattern at distances of 0, 5, and 10 mm.

Fig. S4

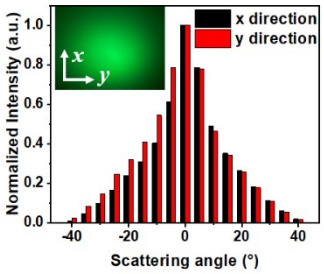

Fig. S4 Normalized scattered light intensity distribution for T-ATW along different directions (inserted photographs of the distribution of scattered light spots for T-ATW).

Fig. S5

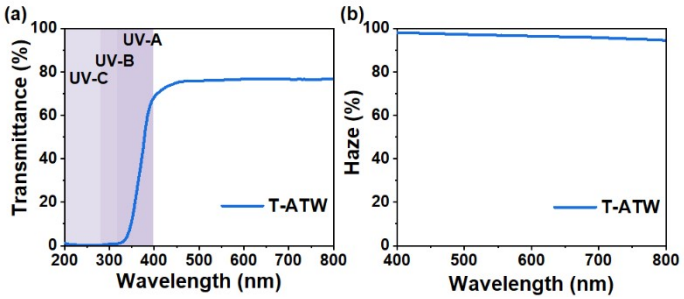

Fig. S5 Total transmittance and haze of T-ATW (thickness= 2 mm).

Fig. S6

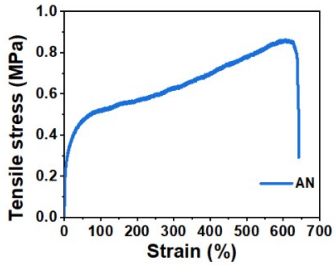

Fig.S6 Tensile stress-strain curve of AN.

Table S2

Table S2 Comparison of the mechanical properties of L-NW, T-NW, L-WS, T-WS, L-ATW, T-ATW, and AN.

	Fracture strength [MPa]	Fracture strain (%)	Elastic modulus [MPa]	Toughness [KJ/m^3]	Flexural strength [MPa]	Flexural strain at break (%)	Work of fracture [KJ/m^3]
L-NW	5.11	1.57	426.65	0.04	17.51	0.92	0.10
T-NW	1.13	1.0	85.17	0.01	1.79	0.97	0.02
L-WS	4.09	1.34	400.78	0.03	12.22	0.87	0.06
T-WS	0.55	0.50	123.43	0.01	-	-	-
L-ATW	13.91	9.74	472.80	0.85	23.62	1.76	0.21
T-ATW	6.47	5.99	199.06	0.25	6.70	3.79	0.84
AN	0.86	609.75	11.53	4.15	-	-	-

Fig. S7

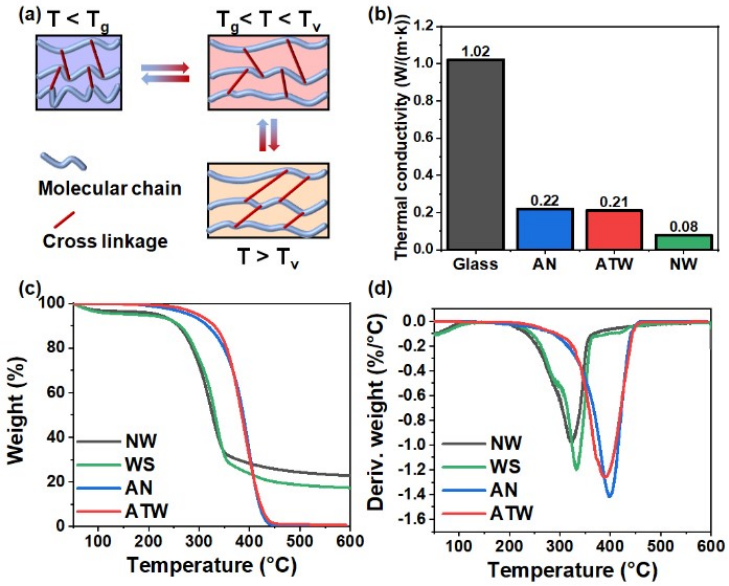

Fig. S7 (a) Exchange reaction scheme of AN. (b) Thermal conductivities of the glass, AN, ATW and NW. (c-d) TG and DTG curves of NW, WS, AN and ATW.

Fig. S8

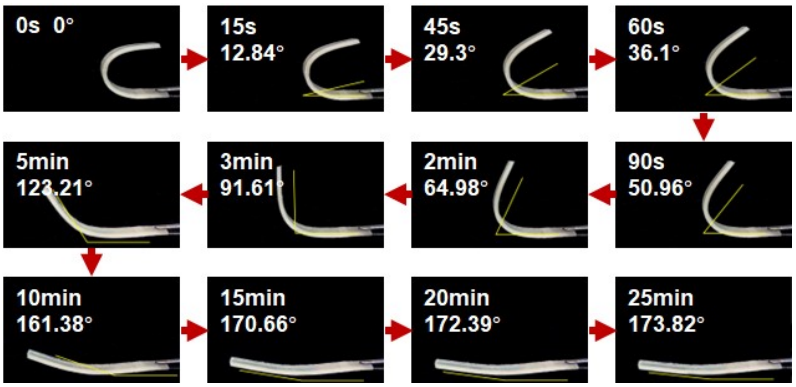

Fig. S8 Photographs of shape recovery performance of ATW at 40 °C within 210 s.

Fig. S9

Fig. S9 Photographs of shape recovery performance of edited ATW at 80 °C within 210 s.

Table S3

Table S2 Comparison of the multi-aspect performances of wood composite and SMW.

Composite materials[a]	Curing condition	Thickness[b] (mm)		Transmittance (%)		Haze (%)		Fracture strength (MPa)		Recovery condition	Ref.
		T[c]	L[c]	T	L	T	L	T	L		
Balsa-MMA	70°C 4 h	-	1.2	-	85	-	70	-	38	-	[7]
Basswood-Epoxy resin	30°C 12 h	3	3	~90	~80	~97	~90	23.38	45.38	-	[4]
SA balsa-MMA	70°C 24 h	2	2	83.8	-	66.9	-	12.8	61.7	-	[8]
MMA-vitrimer composite	100°C 5 h	-	-	-	-	-	-	-	4.96	125 °C	[9]
Balsa-PCL	135°C 4 h	-	-	-	-	-	-	-	10.68	60 °C	[10]
Balsa-Vitrimers	-	-	-	-	-	-	-	-	~21	150 °C	[11]
Balsa-Vitrimers	60°C 12 h	2	2	89.92	70.88	90.99	72.24	8.27	37.24	50 °C	[12]
Balsa-AN	150°C 3 h	2	2	78.91	76.57	94.58	82.63	6.47	9.74	20 °C	This study

a: Composite materials include wood and/or polymer monomer: MMA: Methyl methacrylate; SA: succinic anhydride; PCL: Polycaprolactone.

b: Thickness of samples in the characterization of optical performance.

c: T: Transverse direction; L: Longitudinal direction.

3. Supplementary References

1. H. Khakpour and M. Abdollahi, *J. Polym. Res.*, 2016, **23**, 168.
2. P. H. Madison and T. E. Long, *Biomacromolecules*, 2000, 1, 615-621, **1**, 615-621.
3. U. Azhar, R. Yaqub, H. Li, G. Abbas, Y. Wang, J. Chen, C. Zong, A. Xu, Z. Yabin, S. Zhang and B. Geng, *Arab. J. Chem.*, 2020, **13**, 3801-3816.
4. M. Zhu, J. Song, T. Li, A. Gong, Y. Wang, J. Dai, Y. Yao, W. Luo, D. Henderson and L. Hu, *Adv. Mater.*, 2016, **28**, 5181-5187.
5. Z. Fang, H. Zhu, C. Preston, X. Han, Y. Li, S. Lee, X. Chai, G. Chen and L. Hu, *J. Mater. Chem. C*, 2013, **1**, 6191.
6. Z. Yu, Y. Yao, J. Yao, L. Zhang, Z. Chen, Y. Gao and H. Luo, *J. Mater. Chem. A*, 2017, **5**, 6019-6024.
7. Y. Li, Q. Fu, S. Yu, M. Yan and L. Berglund, *Biomacromolecules*, 2016, **17**, 1358-1364.
8. C. Montanari, P. Olsén and L. A. Berglund, *Green Chem.*, 2020, **22**, 8012-8023.

9. F. Hajiali, S. Tajbakhsh and M. Marić, *Polymer*, 2021, **212**, 123126.
10. L. Wang, B. Luo, D. Wu, Y. Liu, L. Li and H. Liu, *Polymers*, 2019, **11**, 1892.
11. C. Xiong, B. Li, H. Liu, W. Zhao, C. Duan, H. Wu and Y. Ni, *J. Mater. Chem. A*, 2020, **8**, 10898-10908.
12. Y. Tan, K. Wang, Y. Dong, S. Gong, S. Q. Shi and J. Li, *Chem. Eng. J.*, 2022, **448**, 137487.